The Structure of a Quasi-Keplerian Accretion Disk around Magnetized Stars

Isaac Habumugisha[1,2,3] , Edward Jurua[1], Solomon B. Tessema[4], and Anguma K. Simon[5]

[1] Department of Physics, Mbarara University of Science and Technology, Mbarara, Uganda; hisaac08@yaoo.co.uk
[2] Department of Physics, Kabale University, Kabale, Uganda
[3] Department of Physics, Islamic University in Uganda, Mbale, Uganda
[4] Astronomy and Astrophysics Research and Development Department, Entoto Observatory and Research Center, Addis Ababa, Ethiopia
[5] Department of Physics, Muni University, Arua, Uganda

Abstract

In this paper, we present the complete structure of a quasi-Keplerian thin accretion disk with an internal dynamo around a magnetized neutron star. We assume a full quasi-Keplerian disk with the azimuthal velocity deviating from the Keplerian fashion by a factor of ξ $(0 < \xi < 2)$. In our approach, we vertically integrate the radial component of the momentum equation to obtain the radial pressure gradient equation for a thin quasi-Keplerian accretion disk. Our results show that, at large radial distance, the accretion disk behaves in a Keplerian fashion. However, close to the neutron star, pressure gradient force (PGF) largely modifies the disk structure, resulting into sudden dynamical changes in the accretion disk. The corotation radius is shifted inward (outward) for $\xi > 1$ (for $\xi < 1$), and the position of the inner edge with respect to the new corotation radius is also relocated accordingly, as compared to the Keplerian model. The resulting PGF torque couples with viscous torque (when $\xi < 1$) to provide a spin-down torque and a spin-up torque (when $\xi > 1$) while in the advective state. Therefore, neglecting the PGF, as has been the case in previous models, is a glaring omission. Our result has the potential to explain the observable dynamic consequences of accretion disks around magnetized neutron stars.

Key words: accretion, accretion disks – dynamo – stars: neutron – X-rays: binaries

1. Introduction

It is widely agreed that the most successful theoretical model of disk accretion is that of Shakura & Sunyaev (1973). The most crucial result of their model for a disk around a black hole sets the condition for an accretion disk to be thin, i.e., the vertical scale height (H) should be much less than its radial (R) length scale. Thus, the radial component of the pressure gradient is small relative to the stellar radial gravity, and the angular velocity is Keplerian. They also found viscosity to be the main mechanism for angular momentum transfer. On the other hand, angular momentum removal can be magnetic in origin (Ghosh & Lamb 1978).

Accretion disks around magnetized stars greatly influence the stellar magnetic field, which can result in outward angular momentum transfer. Ghosh & Lamb (1979a) presented a detailed model describing the interaction of disk and stellar magnetic field. They pointed out that turbulent motion, reconnection and Kelvin–Helmholtz instability allow the stellar magnetic field to penetrate the disk and regulate the spin of the star (Ghosh & Lamb 1979b). In fact, Ghosh & Lamb (1979a, 1979b) diskovered that the star is spun down beyond the corotation radius, and vice versa. This is due to the impact of a slowly rotating outer part of the accretion disk.

The presence of an intrinsic magnetic field in the accretion disk can enhance the torque acting between an accretion disk and an accreting star (Torkelsson 1998). Tessema & Torkelsson (2010) found a complete solution of a disk structure when the dynamo is included. Their results show that the magnetic field that is produced by the dynamo leads to a significant enhancement of the magnetic torque between the neutron star and the accretion disk, compared to the model by (Ghosh & Lamb 1979a, 1979b). However, they excluded the effect of pressure gradient force (PGF).

Inclusion of the PGF would require a slight deviation from Keplerian motion (Narayan & Yi 1995). This transition results from the internal pressure ($\sim \rho c_s^2$) becoming a significant fraction of the orbital energy. The disk temperatures will be elevated above the values of an unperturbed disk (Campbell & Heptinstall 1998). Thus, a hot, optically thin accretion disk cannot continuously be geometrically thin. In this case, the vertical height $H \sim c_s / \Omega_k$ (Ω_k is the Keplerian angular velocity), implying that $H/R \leqslant 1$ as opposed to $H/R \ll 1$. This is a unique feature of quasi-Keplerian rotation, in that, when the Keplerian radial distances are shifted, the quasi-Keplerian corotation radius and the position of the disk inner edge are shifted inward (Yi et al. 1997).

Consequently, the quasi-Keplerian model may have observable and theoretical interesting results. Hoshi & Shibazaki (1977) considered a quasi-Keplerian model, but they never found a complete accretion disk structure. Later, Yi et al. (1997), who assumed the deviation from Keplerian fashion to be 0.2, diskovered that changes in magnetic torques are marked by a visible change of spin-up or spin-down torque between the disk and neutron star.

In this paper, we seek to find the complete structure of a quasi-Keplerian, dynamo-powered accretion disk around a magnetized slowly rotating neutron star. This model follows the assumptions of Shakura & Sunyaev (1973), i.e., vertical hydrostatic equilibrium, steady state, and the α-parameter for viscosity. Taking up the magnetized compact object model of Wang (1987, 1995), we then modify the Hoshi & Shibazaki (1977) model, using the formulation of Tessema & Torkelsson (2010) while taking into account the effect of radial pressure gradients. We subject our results to the observed data in order to explain such observational scenarios as those in 4U 1728-247 and 4U 1626-67 (Camero-Arranz et al. 2010).

The rest of this paper is structured as follows: Section 2 presents our basic formulation; results (both theoretical and

numerical) are diskussed in Section 3; finally, we present the conclusion of our findings in Section 4.

2. Dynamical Equations

2.1. Model Description

The structure of the disk can be described best if we employ a cylindrical system of coordinates (R, ϕ, z) with the z-axis chosen as the axis of rotation of the neutron star. We consider an optically thick, geometrically thin, axisymmetric ($\partial/\partial\phi = 0$) accretion disk in steady state ($\partial/\partial t = 0$), taking into account the pressure gradient term and the deviation from Keplerian motion for a gas-dominated region of the disk.

In order to study a quasi-Keplerian accretion disk, we introduce a dimensionless variable ξ that shows a deviation from the Keplerian fashion. We assume that the azimuthal velocity is nearly Keplerian, and as a result, values of ξ remain around unity (Campbell 1987) such that $0 < \xi \leqslant 2$ are considered. In the event that $\xi = 1$, we regain the Keplerian form. The azimuthal velocity (v_ϕ) can be modified to

$$v_\phi = \xi\sqrt{\frac{GM}{R}}, \qquad (1)$$

where G is Newton's gravitational constant, M is the mass of the central object, and R is the radius.

2.2. Basic Equations

The basic equations describing the fluid dynamics in a disk calculate the conservation of mass, momentum, and energy, written as:

$$\nabla \cdot (\rho\boldsymbol{v}) = 0, \qquad (2)$$

$$\rho\boldsymbol{v} \cdot \nabla\boldsymbol{v} = -\nabla P - \rho\nabla\Phi + (\boldsymbol{J} \times \boldsymbol{B}) + \rho\nu\nabla^2\boldsymbol{v}, \qquad (3)$$

$$\nabla \cdot [(\rho\varsigma + P) \cdot \boldsymbol{v}] = \boldsymbol{v} \cdot \boldsymbol{f}_\nu - \nabla \cdot \boldsymbol{F}_{\mathrm{rad}} + \frac{\boldsymbol{J}^2}{\sigma} - \nabla \cdot \boldsymbol{q}, \qquad (4)$$

respectively. Here, ρ is the density; $\boldsymbol{v} = (v_R, v_\phi, v_z)$ is the fluid velocity; $\Phi = GM(R^2 + z^2)^{-1/2}$ is the gravitational potential of the central object; $\boldsymbol{J} = (J_R, J_\phi, J_z)$ and $\boldsymbol{B} = (B_R, B_\phi, B_z)$ are the current density and magnetic field with the radial, azimuthal, and vertical components, respectively; ς is the internal energy; $\boldsymbol{f}_\nu$ is the viscous force; $\boldsymbol{F}_{\mathrm{rad}}$ is the radiative energy flux; and ν is the kinematic viscosity. The α-prescription for viscosity is assumed to be (Shakura & Sunyaev 1973),

$$\nu = \alpha_{ss}c_s H, \qquad (5)$$

where α_{ss} is a constant showing the strength of viscosity and $c_s = (P/\rho)^{1/2}$ is the speed of sound. In Equation (4), the term $\frac{\boldsymbol{J}^2}{\sigma}$ is ohmic dissipation and the term $\nabla \cdot \boldsymbol{q}$ is heat conduction. In a quasi-Keplerian motion, the energy balance equation of Frank et al. (2002) is modified to give a relation between temperature and radial distance along the disk:

$$\frac{9}{8}\xi^2\nu\Sigma\frac{GM}{R^3} = \frac{4}{3}\frac{\sigma T_c^4}{\tau}, \qquad (6)$$

where σ is the Stefan–Boltzmann constant, Σ is the surface density, T_c is the temperature at the mid-plane of the disk, and τ is the optical depth of the disk defined using free–free opacity

as given by Kramers' law:

$$\tau = \frac{1}{2}\Sigma\kappa, \qquad (7)$$

where red κ is the Rosseland mean opacity, given by $\kappa = \kappa_0\rho T_c^{-7/2}\,\mathrm{m}^2\,\mathrm{kg}^{-2}\,\mathrm{K}^{-7/2}$ with $\kappa_0 = 5 \times 10^{20}$.

2.3. Ansatz for Magnetic Field

Properties of electromagnetic fields around magnetized, rotating neutron stars have been studied both theoretically (e.g., Bakala et al. 2010; Petri 2013, 2014; Rezzolla et al. 2001) and observationally (e.g., Bildsten et al. 1997). Rezzolla et al. (2001) derived exact general relativistic expressions for the electromagnetic field in the exterior of a rotating neutron star in the approximation of a slow rotation case. They considered a misaligned dipolar stellar magnetic field, but never determined the magnetic torques exerted onto the neutron star. Knowledge of these properties (e.g., length scales, field strength, etc.) benefit our understanding of several astrophysical situations with regard to how the neutron star's magnetosphere interacts with the accretion disk. Lai (1999) considered a non-relativistic but misaligned dipolar magnetic field; they found that the inner region of the accretion disk interacting with the inclined magnetic dipole field is subjected to magnetic torques that induce warping and precession of the disk. The Lai (1999) model is the opposite of Wang (1987), in terms of stellar field alignment and rotation axis. As mentioned in Section 1, we consider a non-relativistic and untilted case for the slowly rotating magnetized neutron star model of Wang (1987, 1995) and then include the dynamo action of Tessema & Torkelsson (2010) as we extend it to a quasi-Keplerian formulation.

In an X-ray binary system, it is difficult for imposed magnetic fields to be compressed to field strengths that are large enough to be dynamically significant in the main part of the disk (Campbell 1987). Consequently, turbulent dynamo action in accretion disks is vital to generate the required magnetic fields (Brandenburg et al. 1995). In the presence of a dynamo mechanism, the stellar field penetrates the disk and a large-scale toroidal field is created with two components: (1) $B_{\phi,\mathrm{shear}}$, which is due to vertical shearing motions (Wang 1987); and (2) $B_{\phi,\mathrm{dyn}}$, which is due to differential rotation (Brandenburg et al. 1995).

The vertical field component, $B_{z,\mathrm{dipole}}$, is assumed to take the form (Wang 1995)

$$B_{z,\mathrm{dipole}} = -\frac{\mu}{R^3}, \qquad (8)$$

where μ is the magnetic dipole moment.

The sheared component of the dipole magnetic field B_z is given by

$$B_{\phi,\mathrm{shear}} = -\gamma B_z\left[1 - \left(\frac{\Omega_s}{\Omega'_k}\right)\right], \qquad (9)$$

where $\Omega'_k = \xi v_\phi/R$ is the angular velocity of the quasi-Keplerian disk. Here, Ω'_k and Ω_k are related in such a way that $\Omega'_k = \xi\Omega_k(R) < \text{or} > \Omega_k(R)$, depending on the value of ξ. We can consider the relation of Ω'_k and Ω_k as:

$$\frac{\Omega'_k}{\Omega_k} = \begin{cases} \xi = 1; & \text{for Keplerian,} \\ 0 < \xi < 2; & \text{for quasi-Keplerian motion.} \end{cases} \qquad (10)$$

In Equation (9), Ω_s is the angular velocity of the star, while $\gamma \gtrsim 1$ (Ghosh & Lamb 1979a) is a dimensionless parameter defined as the ratio of radial distance R to the vertical velocity shear length scale $|v_\phi/(\partial v_\phi/\partial z)|$ (Narayan & Yi 1995). In this case, γ depends on the steepness of the vertical (z-direction) transition between the quasi-Keplerian motion inside the disk and quasi-Keplerian corotation with the star outside the accretion disk, i.e.,

$$B_{\phi,\text{shear}} = \frac{\gamma\mu}{R^3}\left[1 - \frac{1}{\xi}\left(\frac{R}{R'_{\text{co}}}\right)^{3/2}\right]. \quad (11)$$

In this model, $R'_{\text{co}} = \xi^{2/3}R_{\text{co}}$ is the quasi-Keplerian corotation radius where R_{co} is the usual corotation radius expressed as (Tessema & Torkelsson 2010),

$$R_{\text{co}} = \left(\frac{GMP_{\text{spin}}^2}{4\pi^2}\right)^{\frac{1}{3}} = 1.5 \times 10^6 P_{\text{spin}}^{\frac{2}{3}} M_1^{\frac{1}{3}}, \quad (12)$$

where $P_{\text{spin}} = 2\pi/\Omega_s$ is the spin period of the star. Here, M_1 is the ratio $M/M_\odot$, where $M_\odot$ the solar mass.

On the other hand, $B_{\phi,\text{dyn}}$ arising due to dynamo action is expressed as (Tessema & Torkelsson 2011)

$$B_{\phi,\text{dyn}} = \epsilon(\alpha_{\text{ss}}\mu_0\gamma_{\text{dyn}}P(R))^{\frac{1}{2}}, \quad (13)$$

where ϵ is a factor that describes the direction of the magnetic field, μ_0 is the permeability of free space, and $\gamma_{\text{dyn}} = B_\phi/B_R \sim B_\phi/B_z$ (Torkelsson 1998) is the azimuthal pitch. In this case, γ_{dyn} signifies the rate of reconnection and amplification of toroidal field (Campbell 1999). Here, α_{ss} and γ_{dyn} are 0.01 (Shakura & Sunyaev 1973) and 10 (Brandenburg et al. 1995), respectively, while $-1 \leqslant \epsilon \leqslant +1$. The negative value shows a magnetic field that is pointing in the negative ϕ direction at the upper disk surface.

Finally, the radial field component is given by (Lai 1998)

$$B_R = -\frac{B_z}{R}\left(\frac{v_R}{\Omega'_k}\right), \quad (14)$$

which clearly depends on a quasi-Keplerian formulation Ω_k'.

2.4. Disk Structure

The disk structure is fully described by the parameters: pressure, height, density, temperature, and magnetic fields, which are obtained from simplifying the basic equations (Equation (2) and (3)).

The radial component of Equation (2) is expressed as:

$$\frac{1}{R}\frac{\partial}{\partial R}(\rho R v_R) + \frac{\partial}{\partial z}(\rho v_z) = 0. \quad (15)$$

Neglecting vertical outflows, the radial integration of Equation (15) with the appropriate boundary value gives

$$\int_{-H}^{+H}\int_0^{2\pi} \frac{1}{R}\frac{\partial}{\partial R}(\rho R v_R)dzd\phi = 0, \quad (16)$$

leading to the expression for the accretion rate

$$\dot{M} = -2\pi R\Sigma v_R = \text{constant}, \quad (17)$$

where the negative sign shows inflow of matter and $\Sigma = \int_{-H}^{+H}\rho dz = 2\rho H$.

Following the work of Tessema & Torkelsson (2010), the three components of Equation (3) are: radial

$$\rho\left[v_R\frac{\partial v_R}{\partial R} - \frac{v_\phi^2}{R}\right] = -\frac{\partial}{\partial R}\left[P + \frac{\rho GM}{(R^2 + z^2)^{\frac{1}{2}}}\right] + \left[\frac{B_z}{\mu_0}\frac{\partial B_R}{\partial z}\right]$$
$$- \left[\frac{B_z}{\mu_0}\frac{\partial B_z}{\partial R}\right] - \left[\frac{B_\phi}{\mu_0}\frac{1}{R}\frac{\partial(RB_\phi)}{\partial R}\right], \quad (18)$$

azimuthal

$$\rho\left[v_R\frac{\partial v_\phi}{\partial R} + \frac{v_\phi}{R}\right] = \left[\frac{B_R}{\mu_0}\frac{1}{R}\frac{\partial(RB_\phi)}{\partial R}\right] + \left[\frac{B_z}{\mu_0}\frac{\partial B_\phi}{\partial z}\right]$$
$$+ \frac{1}{R^2}\frac{\partial}{\partial R}\left[R^3\rho\nu\frac{\partial}{\partial R}\left(\frac{v_\phi}{R}\right)\right], \quad (19)$$

and vertical

$$\rho\left[v_R\frac{\partial v_z}{\partial R} + v_z\frac{\partial v_z}{\partial z}\right] = -\frac{\partial}{\partial z}\left[P + \frac{\rho GM}{(R^2 + z^2)^{\frac{1}{2}}}\right] + \left[\frac{B_R}{\mu_0}\frac{\partial B_z}{\partial R}\right]$$
$$- \left[\frac{B_\phi}{\mu_0}\frac{\partial B_\phi}{\partial z}\right] - \left[\frac{B_R}{\mu_0}\frac{\partial B_R}{\partial z}\right]. \quad (20)$$

From Equation (20), vertical hydrodynamic equilibrium is expressed as:

$$\frac{\partial}{\partial z}\left(P + \frac{B_R^2 + B_\phi^2}{2\mu_0}\right) = -\rho\frac{GMz}{R^3}. \quad (21)$$

For a relatively high β plasma, thermal pressure will dominate over magnetic pressure. On vertically integrating Equation (21), we get the pressure at the mid-plane of the disk:

$$P(R) = \frac{H\Sigma}{2}\frac{GM}{R^3}. \quad (22)$$

Thus, for a disk dominated by gas pressure, the equation of state for an ideal gas is

$$P(\rho, T_c) = \rho\left(\frac{k_B}{m_p\bar{\mu}}\right)T_c, \quad (23)$$

where k_B is the Boltzmann constant, m_p is the mass of a proton (or the mass of the hydrogen atom m_H, as $m_p \sim m_H$), and $\bar{\mu}$ is the mean molecular weight for the ionized gas. The value of $\bar{\mu}$ ranges between 0.5 for fully ionized hydrogen and 1 for neutral hydrogen (i.e., $0.5 \leqslant \bar{\mu} \leqslant 1$), depending on the degree of ionization of the gas (Frank et al. 2002). In this model, we take $\bar{\mu} = 0.62m_H$, which corresponds to a mixture of ionized gas comprised of 70% hydrogen and 30% helium, by mass. Using Equations (22) and (23), the disk height is given as:

$$H = \left(\frac{m_p\bar{\mu}}{k_B}\right)^{-\frac{1}{2}}\left(\frac{GM}{R^3}\right)^{-\frac{1}{2}}T_c^{\frac{1}{2}}. \quad (24)$$

From the viscous stress tensor, we have

$$\frac{3}{4}\xi(\nu\Sigma)\left(\frac{R^3}{GM}\right)^{-\frac{1}{2}}H^{-1} = \alpha_{ss}P(R). \tag{25}$$

Combining Equations (22), (24), and (25), the density is given by

$$\rho = \frac{3}{4}\xi(\nu\Sigma)\alpha_{ss}^{-1}\left(\frac{GM}{R^3}\right)\left(\frac{m_p\bar{\mu}}{k_B}\right)^{\frac{3}{2}}T_c^{-\frac{3}{2}}. \tag{26}$$

Optical depth of the accretion disk is obtained from

$$\tau = \frac{1}{2}\Sigma\kappa = \rho^2 H\kappa_0 T_c^{-\frac{3}{2}}. \tag{27}$$

Substituting Equations (24) and (26) into Equation (27), the optical density is expressed as:

$$\tau = \frac{9}{16}\xi^2(\nu\Sigma)^2\alpha_{ss}^{-2}\kappa_0\left(\frac{GM}{R^3}\right)^{\frac{3}{2}}\left(\frac{m_p\bar{\mu}}{k_B}\right)^{\frac{5}{2}}T_c^{-6}. \tag{28}$$

The midplane temperature T_c is then obtained from Equation (6):

$$T_c = \left(\frac{243\kappa_0}{512\sigma}\right)^{\frac{1}{10}}\left(\frac{GM}{R^3}\right)^{\frac{1}{4}}\left(\frac{m_p\bar{\mu}}{k_B}\right)^{\frac{1}{4}}\alpha_{ss}^{-\frac{1}{5}}\xi^{\frac{2}{5}}(\nu\Sigma)^{\frac{3}{10}}. \tag{29}$$

From Equation (22), we can obtain a pressure expression that is related to R:

$$P(R) = \frac{3}{4}\left(\frac{243\kappa_0}{512\sigma}\right)^{-\frac{1}{20}}\left(\frac{GM}{R^3}\right)^{\frac{7}{8}}\left(\frac{m_p\bar{\mu}}{k_B}\right)^{\frac{3}{8}}\alpha_{ss}^{-\frac{9}{10}}\xi^{\frac{4}{5}}(\nu\Sigma)^{\frac{17}{20}}. \tag{30}$$

Surface density Σ and radial velocity v_R take the form:

$$\Sigma = \frac{3}{2}\left(\frac{243\kappa_0}{512\sigma}\right)^{-\frac{1}{10}}\left(\frac{GM}{R^3}\right)^{\frac{1}{4}}\left(\frac{m_p\bar{\mu}}{k_B}\right)^{\frac{3}{4}}\alpha_{ss}^{-\frac{4}{5}}\xi^{\frac{2}{5}}(\nu\Sigma)^{\frac{7}{10}}, \tag{31}$$

and

$$v_R = -\frac{\dot{M}}{3\pi}\left(\frac{243\kappa_0}{512\sigma}\right)^{\frac{1}{10}}\left(\frac{m_p\bar{\mu}}{k_B}\right)^{-\frac{3}{4}}(GM)^{-\frac{1}{4}}\alpha_{ss}^{\frac{4}{5}}\xi^{-\frac{2}{5}}(\nu\Sigma)^{-\frac{7}{10}}R^{-\frac{1}{4}}. \tag{32}$$

This layout provides a basis to find the complete structure of a quasi-Keplerian accretion disk.

3. Results and Discussion

3.1. Global Solutions

All structural equations appear as a function of $\nu\Sigma$. This can be made explicit from the azimuthal component of momentum equation (Equation (19)) by integrating vertically, which yields:

$$\Sigma\left[v_R\frac{\partial\ell}{\partial R}\right] = R\left[\frac{B_z B_\phi}{\mu_0}\right]_{z=-H}^{z=+H} + \frac{1}{R}\frac{\partial}{\partial R}\left[R^3(\nu\Sigma)\frac{\partial}{\partial R}\left(\frac{\ell}{R^2}\right)\right], \tag{33}$$

where $\ell = Rv_\phi$ is the specific angular momentum. Here, we have eliminated the term in $\left[\frac{B_R}{\mu_0}\frac{1}{R}\frac{\partial(RB_\phi)}{\partial R}\right]$ due to spatial difference. Taking $B_{\phi,\text{dyn}}B_{z,\text{dipole}}$ and $B_{\phi,\text{shear}}B_{z,\text{dipole}}$ as the

dominant terms (Tessema & Torkelsson 2010) of the expansion for $B_z B_\phi$ term in Equation (33), we have

$$\Sigma\left[v_R\frac{\partial\ell}{\partial R}\right] = 2R[B_z(B_{\phi,\text{dyn}} + B_{\phi,\text{shear}})]$$
$$+ \frac{1}{R}\frac{\partial}{\partial R}\left[R^3(\nu\Sigma)\frac{\partial}{\partial R}\left(\frac{\ell}{R^2}\right)\right], \tag{34}$$

Using equations (Equations (1), (8), (11), (13), and (17)) in Equation (34), we have

$$y' = \frac{\dot{M}}{6\pi R}\xi^{-\frac{2}{5}} - \frac{y}{2R} - C_1\epsilon\xi^{-\frac{3}{5}}y^{\frac{17}{40}}R^{-\frac{45}{16}}$$
$$- C_2\xi^{-1}R^{-\frac{9}{2}}\left[1 - \frac{1}{\xi}\left(\frac{R}{R_{\text{co}}}\right)^{\frac{3}{2}}\right], \tag{35}$$

where $C_1 = \left[\left(\frac{4}{3}\frac{\gamma_{\text{dyn}}}{\mu_0}\right)^{\frac{1}{2}}\left(\frac{243\kappa_0}{512\sigma}\right)^{-\frac{1}{40}}\left(\frac{m_p\bar{\mu}}{k_B}\right)^{\frac{3}{16}}\mu\alpha_{ss}^{\frac{20}{20}}(GM)^{-\frac{1}{16}}\right]$ and $C_2 = \frac{4}{3}\frac{\mu^2}{\mu_0}\gamma(GM)^{-\frac{1}{2}}$. This is a differential equation in y for the quasi-Keplerian case, which is analogous to Equation (41) of Tessema & Torkelsson (2010) only when the value of $\xi = 1$.

We need to transform Equation (35) by introducing dimensionless quantities, Λ and r, so that

$$y = \Lambda\dot{M} \tag{36}$$

$$R = rR_A. \tag{37}$$

Here, r is a dimensionless radial coordinate and R_A is the Alfvén radius, which is a characteristic radius at which magnetic stresses dominate the flow in the accretion disk. It is obtained by equating the magnetic pressure to the ram pressure (Frank et al. 2002).

$$R_A = \left(\frac{2\pi^2\mu^4}{GM\dot{M}^2\mu_0^2}\right)^{\frac{1}{7}} = 5.1\times10^6\dot{M}_{13}^{-\frac{2}{7}}M_1^{-\frac{1}{7}}\mu_{20}^{\frac{4}{7}}\text{m}, \tag{38}$$

where $\dot{M}$ is the rate of accretion, μ_{20} is the stellar magnetic dipole moment in units of $10^{20}\,\text{Tm}^3$, and $\dot{M}_{13}$ is the accretion rate in units of $10^{13}\,\text{kg s}^{-1}$.

Finally, we get a differential equation in Λ as:

$$\Lambda' = \frac{1}{6\pi r}\xi^{-\frac{2}{5}} - \frac{\Lambda}{2r} - C_3\epsilon\xi^{-\frac{3}{5}}\Lambda^{\frac{17}{40}}r^{-\frac{45}{16}}$$
$$- C_4\xi^{-1}r^{-\frac{9}{2}}\left[1 - \frac{\omega_s}{\xi}r^{\frac{3}{2}}\right], \tag{39}$$

where $C_3 = C_1\dot{M}^{\frac{17}{40}}R_A^{-\frac{45}{16}}$, $C_4 = C_2R_A^{-\frac{9}{16}}$, and ω_s is a fastness parameter defined as (Elsner & Lamb 1977), $\omega_s = (R_A/R_{\text{co}})^{\frac{3}{2}} = 6.3M_1^{-\frac{5}{7}}\dot{M}_{13}^{-\frac{3}{7}}\mu_{20}^{\frac{6}{7}}P^{-1}$. Equation (39) is the new analytical solution for a quasi-Keplerian model. In the limit $\omega_s < 1$, steady accretion takes place, while for $\omega_s > 1$, accretion is unsteady and the accreting matter will be propelled outward by centrifugal forces. We also note that, as $r\to\infty$(say, $100R_A$), then $\Lambda\to1/3\pi$, which becomes the boundary condition for this model.

In the absence of a magnetic field ($\gamma = 0$), internal dynamo ($\gamma_{\text{dyn}} = 0$), and the quasi-Keplerian assumption ($\xi = 1$), the

expression for Λ reduces to

$$\frac{d\Lambda}{dr} = -\frac{\Lambda}{2r} + \frac{1}{6\pi r}, \qquad (40)$$

which is similar to the Shakura–Sunyaev (SS) model equation, originally derived by Shakura & Sunyaev (1973), in the classical model around black holes in binary system.

Close examination of Equation (39) shows that there are two possible boundary conditions to locate the inner edge of the disk. We can define them as Case D and Case V (Tessema & Torkelsson 2010). First, in Case D, the inner edge is located at a radial distance where the density and temperature drop to zero as the inflow velocity becomes infinite, meaning that $\Lambda = 0$ (Shakura & Sunyaev 1973). Second, in Case V, the inner edge is located at a radial distance where the disk plasma is driven along field lines by transfer of excess angular momentum (Wang 1995). In this case, $\Lambda \neq 0$.

In our model, we consider a neutron star that is accreting at a rate of 10^{13} kg s^{-1}, with a mass $M = 1.4 \, M_\odot$ and a magnetic moment of 10^{20} Tm^3. We fix the parameters α_{ss}, γ and γ_{dyn} to 0.01, 1, and 10, respectively. Throughout our work, we set the quasi-Keplerian parameter ξ to 0.8 and 1.2, because azimuthal velocity is close to Keplerian. This will enable us observe the behavior of the disk as it transits to and from Keplerian fashion with the azimuthal velocity varying by 20% below and above the Keplerian azimuthal velocity. The spin periods of interest in this model are 7 and 100 s, and we obtain a solution for each spin period while changing the dynamo parameter to $\epsilon = 1.0$, 0.1, 0, -0.1, and -1. These spin periods were deliberately chosen because they cover a wide range of slowly rotating stars that exhibit torque reversals, e.g., 4U 1626-67 (Period = 7.6 s) and 4U 1728-247 (Period = 120 s) (Bildsten et al. 1997; Camero-Arranz et al. 2010).

On the other hand, rapid rotators such as SAX J1808.4-3658 have also been observed to have spin variations (Burderi et al. 2006) that can be explained best in a dynamo model (Tessema & Torkelsson 2011). They behave uniquely when the accreting plasma is threaded by the stellar magnetic field (Naso & Miller 2010, 2011). To find a complete structure of such a disk, the disk is divided into regions depending on the equation of state. For example, the SS model solution considers the regions of the disk to have pressure either dominated by radiation pressure or ideal gas pressure, and the main opacity source is electron scattering or Kramers' opacity (Shakura & Sunyaev 1973, 1976). However, to analyze the dynamics of a quasi-Keplerian accretion disk, we focus here on a gas-pressure-dominated disk around a slowly rotating magnetized neutron star.

The global solutions show that, at large radial distance, both Keplerian and quasi-Keplerian motion exhibit nearly the same Λ variations with radius (Figure 1). As the quasi-Keplerian disk interacts with the star's magnetosphere, the corotation radius is shifted inward for $\Omega'_k > \Omega_k$ and outward for $\Omega'_k < \Omega_k$. Subsequently, the position of the inner edge with respect to the new corotation radius is relocated. When $\Omega'_k > \Omega_k > \Omega_s$ ($\Omega'_k < \Omega_k < \Omega_s$), the disk plasma is moving faster (slower) than the star; consequently, magnetic stresses act to spin up (down) the star (Wang 1995). Further, we note that varying the quasi-Keplerian parameters modifies the disk structure and the star consequently experiences enhanced torques. In previous studies, quasi-Keplerianity has been

restricted to only when $\Omega'_k < \Omega_k$ (Narayan & Yi 1995). This study explored both situations.

Figure 1 shows the variation of Λ as a function of r for both $P = 7$ s and $P = 100$ s. All $\epsilon = 1.0$, 0.1, and 0 solutions are case V inner boundaries, in addition to $\epsilon = -0.1$ for $P = 100$ s when $\xi = 1.0$ and $\xi = 1.2$; see Figure 2. For $P = 7$ s, the local minimum that occurs when $\epsilon = 0$ keeps disappearing as the disk reaches a quasi-Keplerian state (Figure 1) top panel. In this transition, the dynamo substantially influences the nature of the global solution. Dynamo action was found to result in enhanced magnetic torques between the star and disk (Tessema & Torkelsson 2010). Therefore, a combination of dynamo action and quasi-Keplerian situation has an effect on torque reversal. We believe that this is a possible physical situation that arises in an accretion disk at an inner radius so close to the neutron star.

3.2. The Structure of a Quasi-Keplerian Disk

The structural equations are obtained by expressing all the unknowns P, T_c, H/R, Σ, ρ, τ, ν, v_R, $B_{\phi,\text{dyn}}$, and B_R, in terms of α_{ss}, $\dot{M}_{13}$, M_1, μ_{20}, $\bar{\mu}$, $\Lambda(r)$, and r, obtained as:

$$\Sigma = 3.8 \times 10^3 \alpha_{ss}^{-\frac{4}{5}} \xi^{\frac{2}{5}} \bar{\mu}^{\frac{3}{4}} \mu_{20}^{-\frac{3}{7}} \dot{M}_{13}^{\frac{32}{35}} M_1^{\frac{5}{14}} \Lambda(r)^{\frac{7}{10}} r^{-\frac{3}{4}} \text{ kg m}^{-2} \qquad (41)$$

$$\rho = 3.0 \times 10^{-2} \alpha_{ss}^{-\frac{7}{10}} \xi^1 \bar{\mu}^{\frac{9}{8}} \mu_{20}^{-\frac{15}{14}} \dot{M}_{13}^{\frac{38}{35}} M_1^{\frac{25}{28}} \Lambda(r)^{\frac{11}{20}} r^{-\frac{15}{8}} \text{ kg m}^{-3} \qquad (42)$$

$$P = 1.2 \times 10^8 \alpha_{ss}^{-\frac{9}{10}} \xi^{\frac{4}{5}} \bar{\mu}^{\frac{3}{8}} \mu_{20}^{-\frac{3}{2}} \dot{M}_{13}^{\frac{8}{5}} M_1^{\frac{5}{4}} \Lambda(r)^{\frac{17}{20}} r^{-\frac{21}{8}} \text{ N m}^{-2} \quad (43)$$

$$\nu = 4.0 \times 10^9 \alpha_{ss}^{\frac{4}{5}} \xi^{\frac{1}{5}} \bar{\mu}^{-\frac{3}{4}} \mu_{20}^{\frac{3}{7}} \dot{M}_{13}^{\frac{3}{35}} M_1^{-\frac{5}{14}} \Lambda(r)^{\frac{3}{10}} r^{\frac{3}{4}} \text{ m}^2 \text{ s}^{-1} \quad (44)$$

$$T_c = 4.8 \times 10^5 \alpha_{ss}^{-\frac{1}{5}} \xi^{\frac{2}{5}} \bar{\mu}^{\frac{1}{4}} \mu_{20}^{-\frac{3}{7}} \dot{M}_{13}^{\frac{18}{35}} M_1^{\frac{5}{14}} \Lambda(r)^{\frac{3}{10}} r^{-\frac{3}{4}} \text{ K} \qquad (45)$$

$$\frac{H}{R} = 1.2 \times 10^{-2} \alpha_{ss}^{-\frac{1}{10}} \xi^{\frac{1}{5}} \bar{\mu}^{-\frac{3}{8}} \mu_{20}^{\frac{1}{14}} \dot{M}_{13}^{-\frac{4}{35}} M_1^{-\frac{11}{28}} \Lambda(r)^{\frac{3}{20}} r^{\frac{1}{8}} \quad (46)$$

$$v_R = 82.8 \alpha_{ss}^{\frac{4}{5}} \xi^{-\frac{2}{5}} \bar{\mu}^{-\frac{3}{4}} \mu_{20}^{-\frac{1}{7}} \dot{M}_{13}^{\frac{13}{35}} M_1^{-\frac{1}{14}} \Lambda(r)^{-\frac{7}{10}} r^{-\frac{1}{4}} \text{ m s}^{-1} \quad (47)$$

$$\tau = 3.63 \times 10^2 \alpha_{ss}^{-\frac{4}{5}} \xi^2 \bar{\mu} \, \dot{M}_{13}^{\frac{1}{5}} \Lambda(r)^{\frac{1}{5}} \qquad (48)$$

$$B_{\phi,\text{shear}} = 0.75 \gamma \mu_{20}^{-\frac{5}{7}} \dot{M}_{13}^{\frac{6}{7}} M_1^{\frac{3}{7}} r^{-3} (1 - \omega_s \xi^{-1} r^{3/2}) \text{ T} \qquad (49)$$

$$B_{\phi,\text{dyn}} = 12.0 \epsilon \alpha_{ss}^{\frac{1}{20}} \xi^{\frac{2}{5}} \gamma_{\text{dyn}}^{\frac{1}{2}} \bar{\mu}^{\frac{1}{16}} \mu_{20}^{-\frac{3}{4}} \dot{M}_{13}^{\frac{4}{5}} M_1^{\frac{5}{8}} \Lambda(r)^{\frac{17}{40}} r^{-\frac{21}{16}} \text{ T} \quad (50)$$

$$B_R = 1.2 \times 10^{-5} \alpha_{ss}^{\frac{4}{5}} \xi^{-\frac{7}{5}} \bar{\mu}^{-\frac{3}{4}} \mu_{20}^{-\frac{4}{7}} \dot{M}_{13}^{\frac{38}{35}} M_1^{-\frac{5}{14}} \Lambda(r)^{\frac{-7}{10}} \xi^{-1} r^{-\frac{11}{4}} \text{ T}. \qquad (51)$$

It is easy to see that, when $\xi = 1$, we regain the Keplerian form. We now present a comparison between quasi-Keplerian and Keplerian structural equation solutions.

In Figure 3, we run surface density for spin periods $P = 7$ and 100 s for a changing dynamo parameter of $\epsilon = -1$, 0, 1.

(a)$\xi = 0.8$ (b)$\xi = 1.0$ (c)$\xi = 1.2$

(d)$\xi = 0.8$ (e)$\xi = 1.0$ (f)$\xi = 1.2$
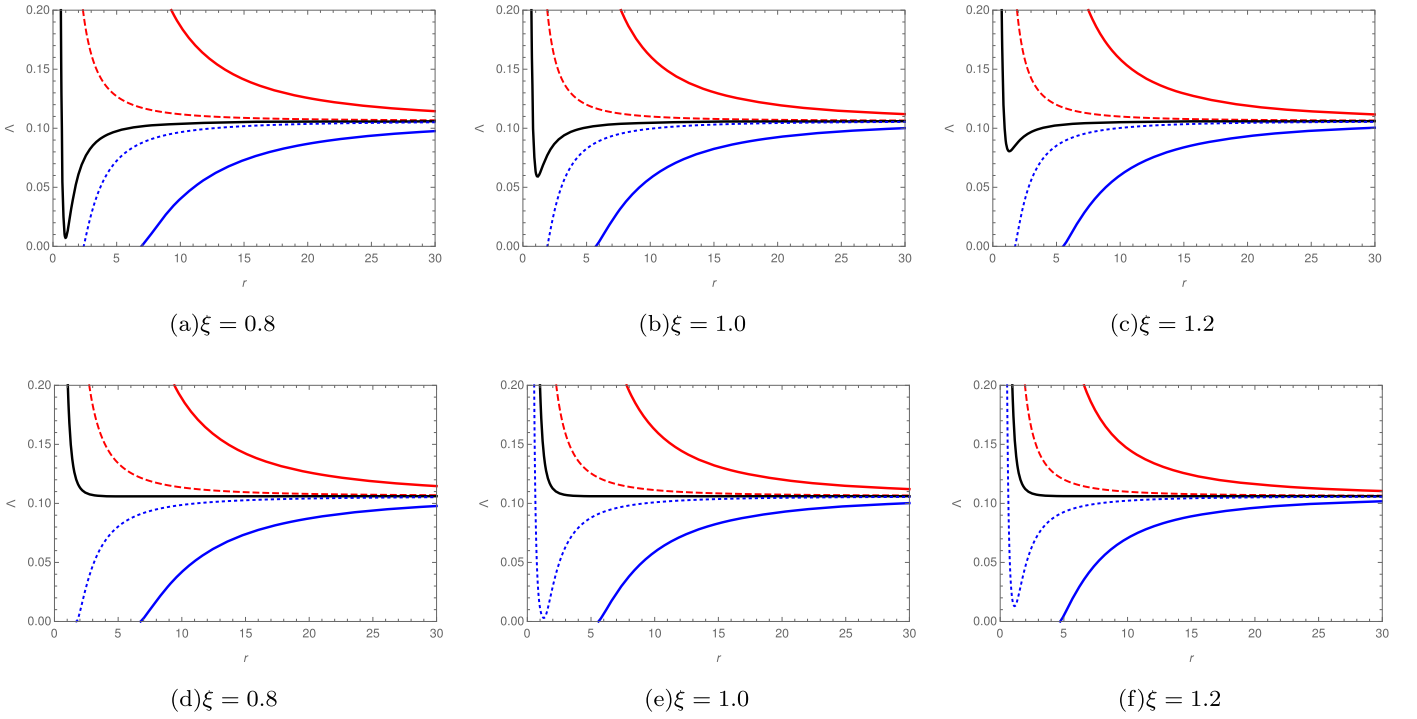
Figure 1. Variation of $\Lambda(r)$ with radial distance for a neutron star with a spin period of 7 s (top panel) or 100 s (bottom panel). The magnetic fields generated by the dynamo are shown with: $\epsilon = -1.0$ blue thick, $\epsilon = -0.1$ blue dotted, $\epsilon = 0$ black, $\epsilon = 0.1$ red dashed, and $\epsilon = 1.0$ red thick lines.
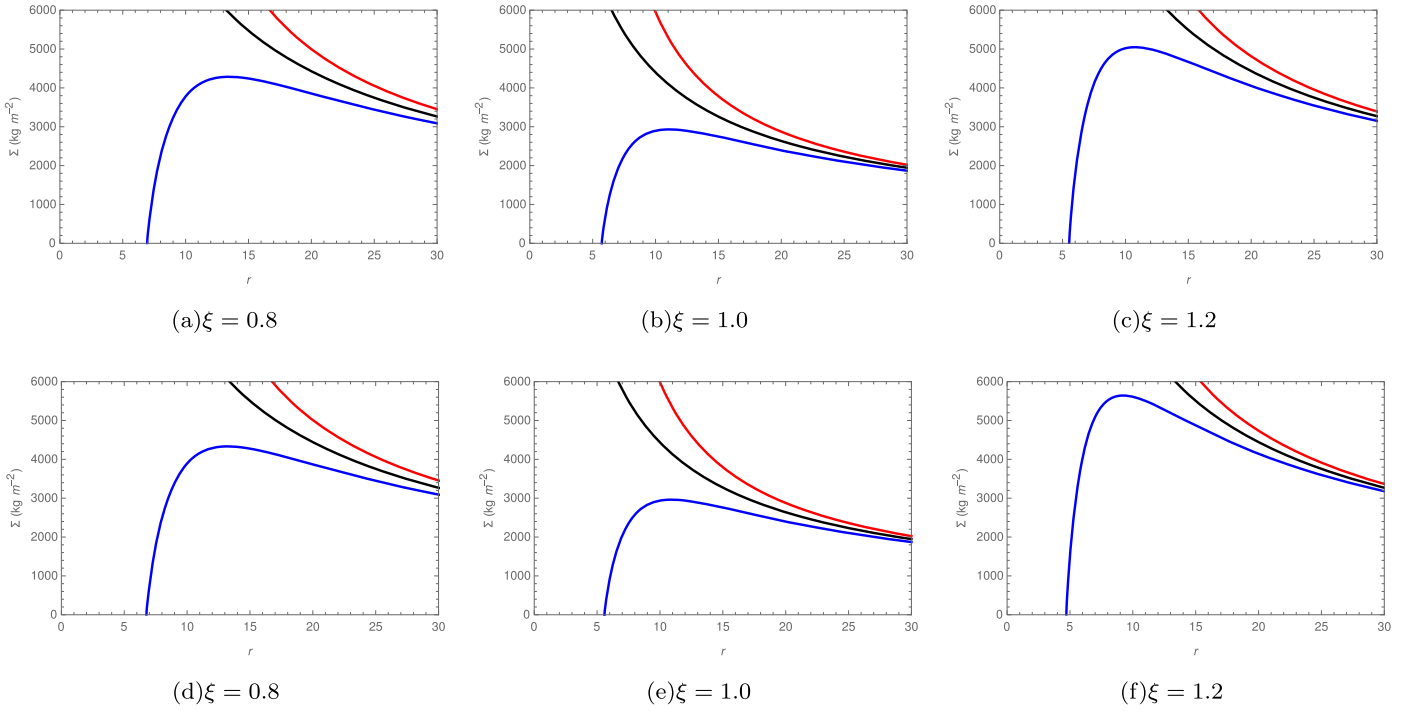

(a)$\xi = 0.8$ (b)$\xi = 1.0$ (c)$\xi = 1.2$

(d)$\xi = 0.8$ (e)$\xi = 1.0$ (f)$\xi = 1.2$
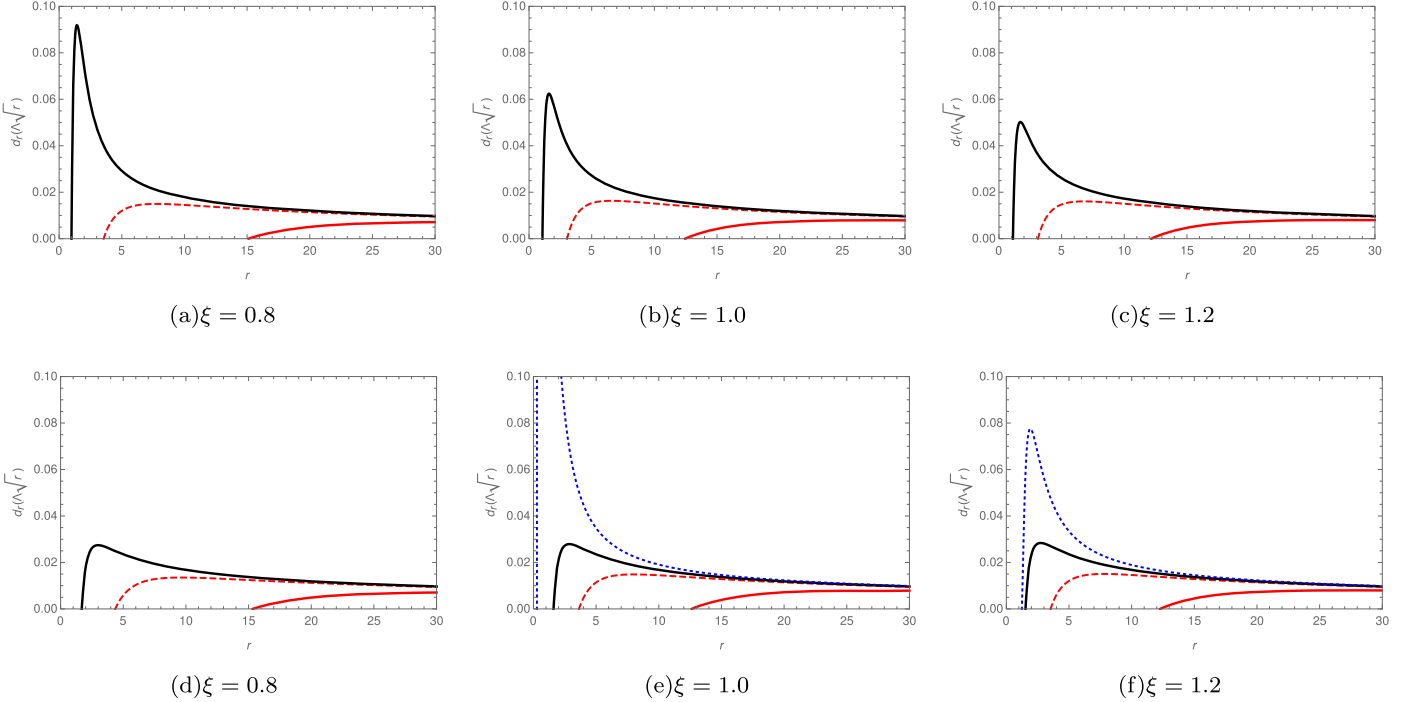
Figure 2. Variation of $\frac{d}{dr}(\sqrt{r}\,\Lambda(r))$ with radial distance for a neutron star with a spin period of 7 s (top panel) or 100 s (bottom panel). The magnetic fields generated by the dynamo are shown with: $\epsilon = -1.0$ blue thick, $\epsilon = -0.1$ blue dotted, $\epsilon = 0$ black, $\epsilon = 0.1$ red dashed, and $\epsilon = 1.0$ red thick lines.

For $\xi = 1.0$, our results correspond to those of Tessema & Torkelsson ([2010](#)). Closer to the neutron star, surface density is a purely decreasing function of r for $\epsilon = 0$ and 1. With $\epsilon = -1$, $\Sigma(r)$ develops a local maximum that is observed to increase for $\xi = 1.2$ and to decrease for $\xi = 0.8$. The local maximum for either period as the disk deviates from Keplerian motion has no significant change. The high surface density, $\xi = 1.2$, results into a hot flow (Figure [4](#)) and a corresponding drop in radial velocity (Figure [5](#))—thus creating pressure gradients.

Figure [6](#) shows the toroidal field's variation with radial distance. Here, as the disk transits to quasi-Keplerianity, the magnitude of the toroidal field increases. Thus, deviation from

(a)$\xi = 0.8$ (b)$\xi = 1.0$ (c)$\xi = 1.2$

(d)$\xi = 0.8$ (e)$\xi = 1.0$ (f)$\xi = 1.2$

Figure 3. Variation of $\Sigma(r)$ with radial distance for a neutron star with a spin period of 7 s (top panel) or 100 s (bottom panel). The magnetic fields generated by the dynamo are shown with: $\epsilon = -1.0$ blue thick, $\epsilon = 0$ black, and $\epsilon = 1.0$ red thick lines.

(a)$\xi = 0.8$ (b)$\xi = 1.0$ (c)$\xi = 1.2$

(d)$\xi = 0.8$ (e)$\xi = 1.0$ (f)$\xi = 1.2$
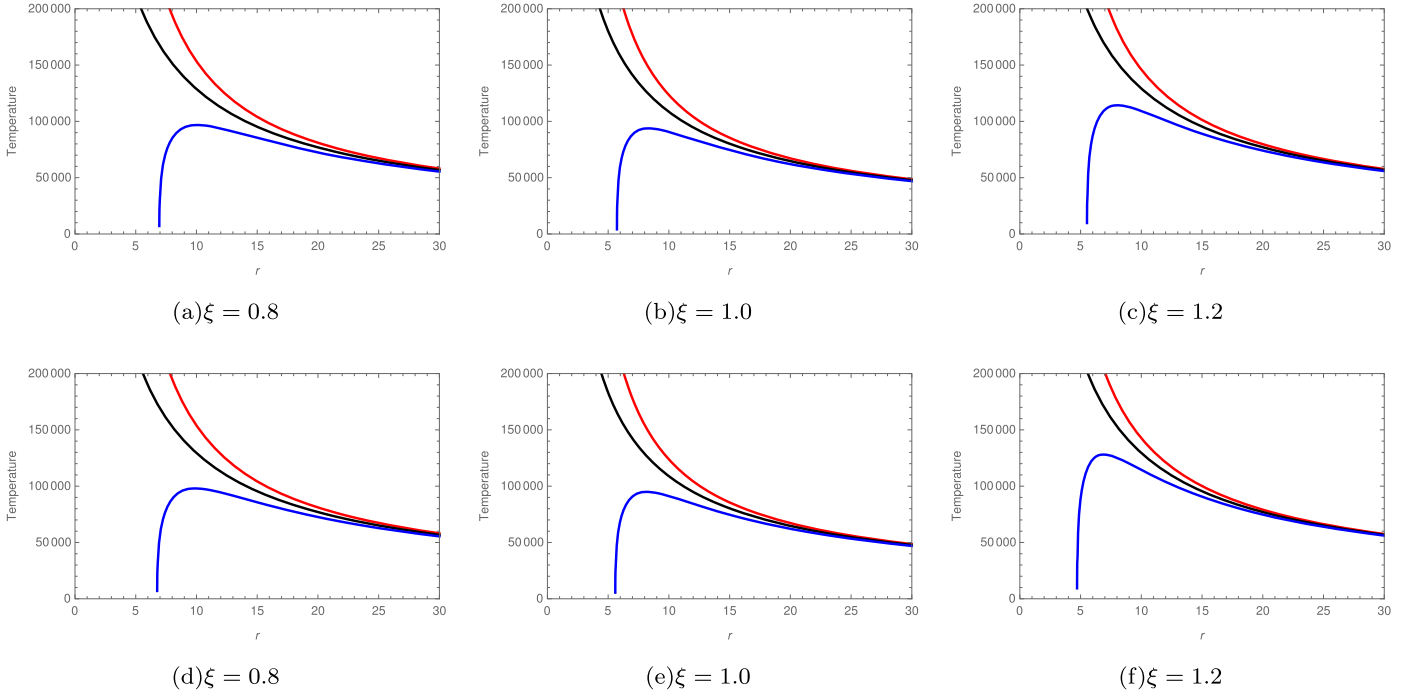
Figure 4. Variation of temperature with radial distance for a neutron star with a spin period of 7 s (top panel) or 100 s (bottom panel). The magnetic fields generated by the dynamo are shown with: $\epsilon = -1.0$ blue thick, $\epsilon = 0$ black, and $\epsilon = 1.0$ red thick lines.

Keplerian motion has a significant impact on the magnitude of magnetic torques on the neutron star.
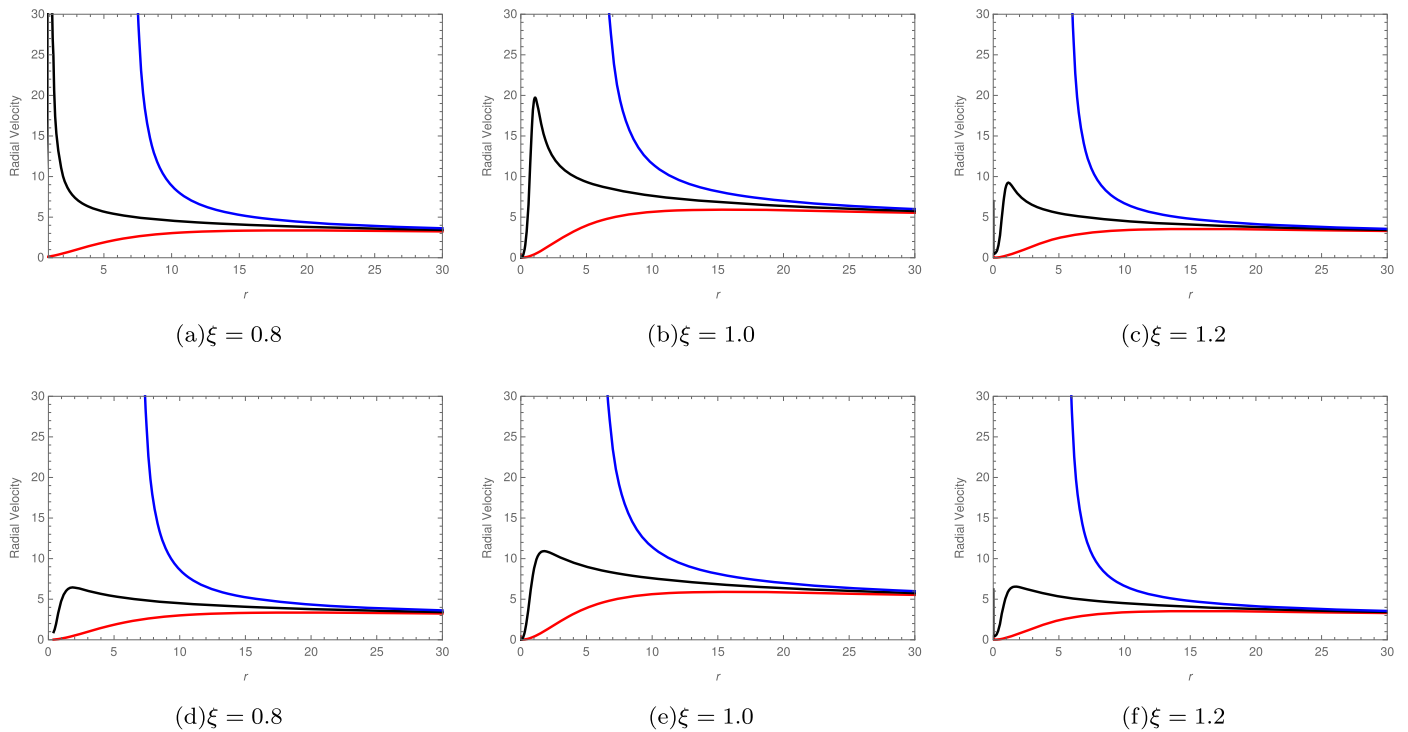
3.3. Effect of PGF

In this section, we analyze the effect of PGF on a case where gas pressure dominates. We obtain the pressure gradient equation by vertically integrating Equation (18) to get

$$\frac{\partial \Pi}{\partial R} = -\Sigma \left[v_R \frac{\partial v_R}{\partial R} - \frac{v_\phi^2}{R} \right] - \frac{\Sigma GM}{R^2} + \left[\frac{B_z B_R}{\mu_0} \right]_{z=-H}^{z=+H}, \quad (52)$$

where $\Pi = \int_{-H}^{+H} P \, dz$ and $B_R|_{z=-H} = -B_R|_{z=+H}$. Here, $B_R|_{z=+H}$ means that B_R is evaluated in the upper disk plane.

(a)$\xi = 0.8$ (b)$\xi = 1.0$ (c)$\xi = 1.2$

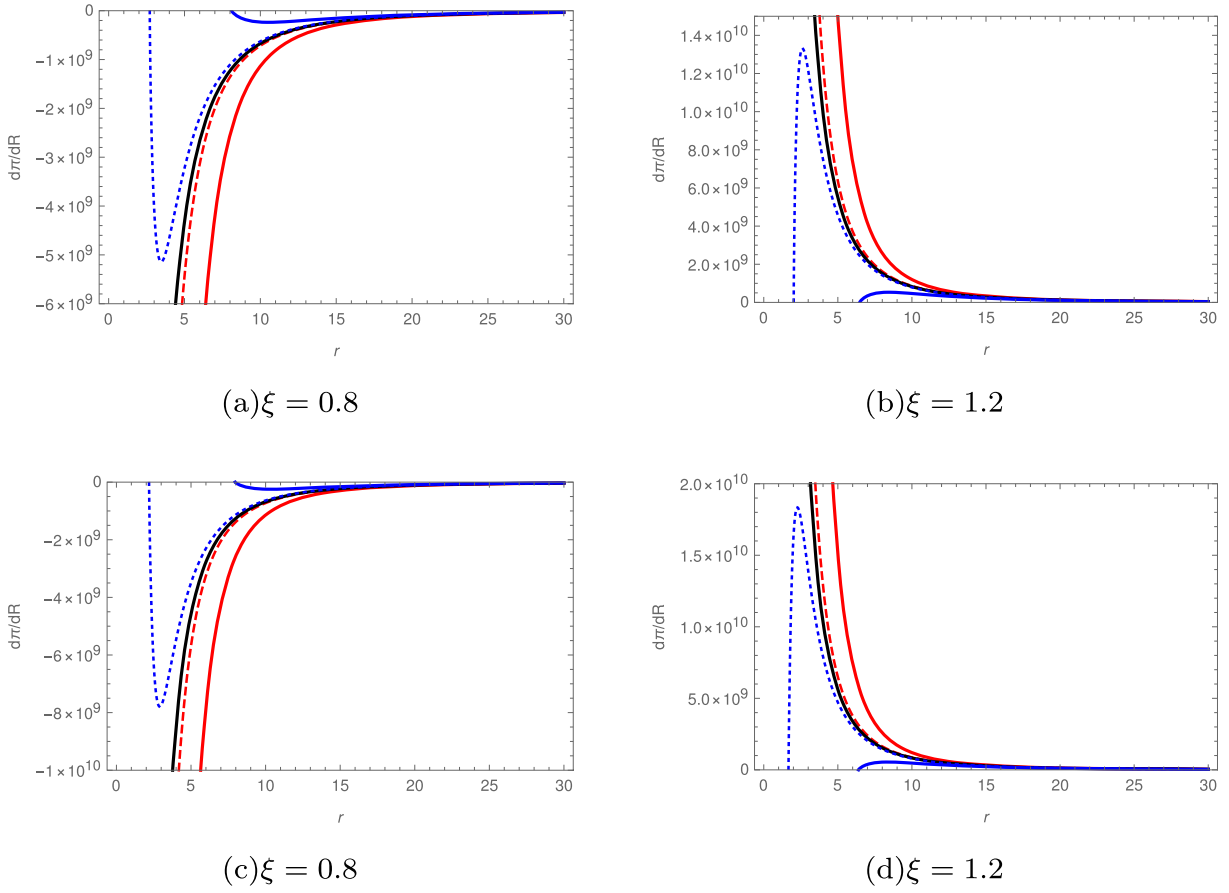(d)$\xi = 0.8$ (e)$\xi = 1.0$ (f)$\xi = 1.2$

Figure 5. Variation of $V_R(r)$ with radial distance for a neutron star with a spin period of 7 s (top panel) or 100 s (bottom panel). The magnetic fields generated by the dynamo are shown with: $\epsilon = -1.0$ blue thick, $\epsilon = 0$ black, and $\epsilon = 1.0$ red thick lines.

(a)$\xi = 0.8$ (b)$\xi = 1.0$ (c)$\xi = 1.2$

(d)$\xi = 0.8$ (e)$\xi = 1.0$ (f)$\xi = 1.2$
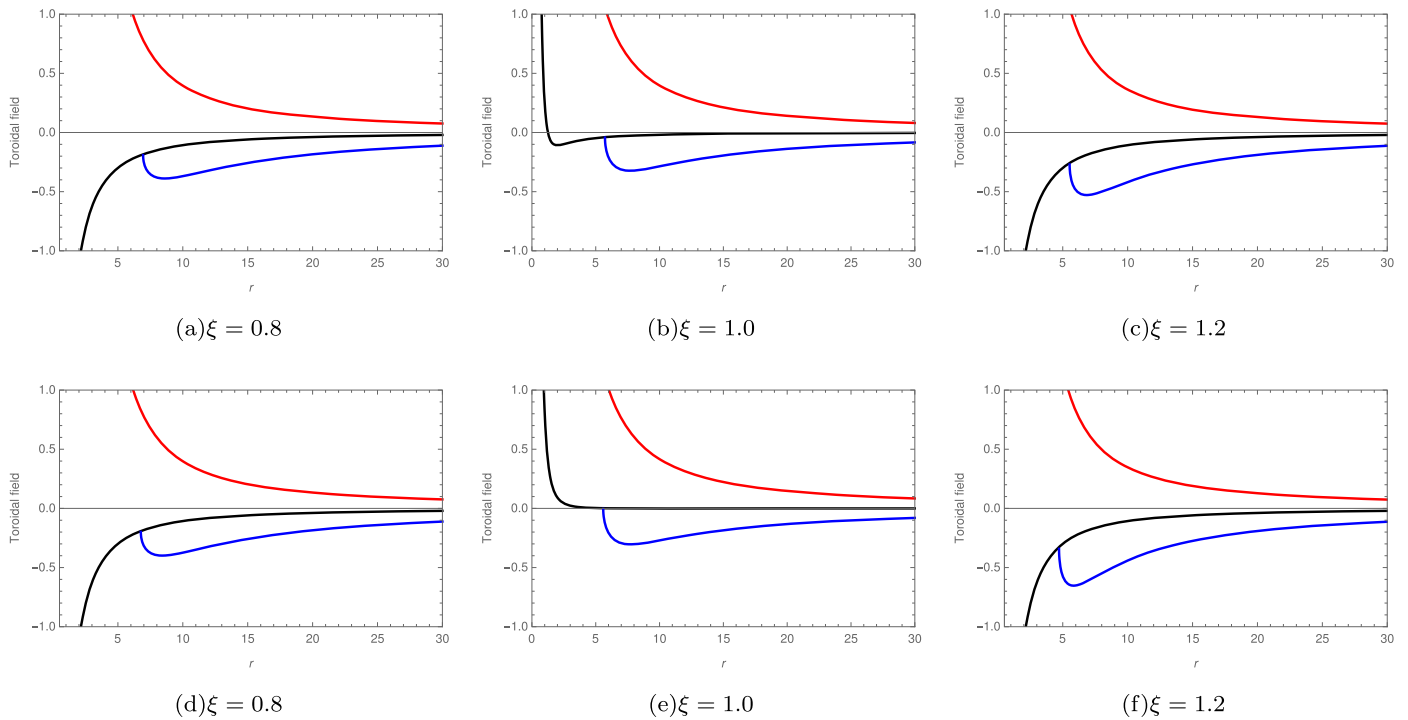
Figure 6. Variation of toroidal field with radial distance for a neutron star with a spin period of 7 s (top panel) or 100 s (bottom panel). The magnetic fields generated by the dynamo are shown with: $\epsilon = -1.0$ blue thick, $\epsilon = 0$ black, and $\epsilon = 1.0$ red thick lines.

Figure 7. Pressure gradient force ($\partial\Pi/\partial R$) as a function of radial distance for a neutron star with a spin period of 7.0 s (top panel (a) and (b)) or 100 s (bottom panel (c) and (d)). The magnetic fields generated by the dynamo are shown with: $\epsilon = -1.0$ blue thick, $\epsilon = -0.1$ blue dotted, $\epsilon = 0$ black, $\epsilon = 0.1$ red dashed, and $\epsilon = 1.0$ red thick lines.

The third term on the right-hand side represents dominant radial magnetic force. Using Equations (1), (14), (8), and (17) in Equation (52), we obtain

$$\frac{\partial\Pi}{\partial R} = \Sigma(\xi^2 - 1)\frac{GM}{R^2} + \left(\frac{\dot{M}}{2\pi}\right)^2\left[\frac{\Sigma^{-1}}{R^3} - \frac{1}{R^2}\frac{\partial\Sigma^{-1}}{\partial R}\right]$$
$$+ \left(\frac{\dot{M}}{\pi}\right)\left[\frac{\mu^2}{\mu_0}\xi^{-1}\Sigma^{-1}(GM)^{-\frac{1}{2}}R^{-\frac{13}{2}}\right]. \quad (53)$$

Transforming and simplifying Equation (53) yields:

$$\frac{\partial\Pi}{\partial R} = D_1(\xi^2 - 1)\Lambda(r)^{\frac{7}{10}}r^{-\frac{11}{4}} + D_2\Lambda(r)^{-\frac{7}{10}}r^{-\frac{9}{4}}$$
$$+ D_3\xi^{-1}\Lambda(r)^{-\frac{7}{10}}r^{-\frac{23}{4}}, \quad (54)$$

where $D_1 = \left[\frac{3}{2}\left(\frac{243\kappa_0}{512\sigma}\right)^{-\frac{1}{10}}\alpha_{ss}^{-\frac{4}{5}}\left(\frac{k_B}{\bar{\mu}m_p}\right)^{-\frac{3}{4}}(GM)^{\frac{5}{4}}\dot{M}^{\frac{7}{10}}R_A^{-\frac{11}{4}}\right]$, $D_2 =$ $\left[\frac{1}{4\pi^2}\left(\frac{243\kappa_0}{512\sigma}\right)^{\frac{1}{10}}\alpha_{ss}^{\frac{4}{5}}\left(\frac{k_B}{\bar{\mu}m_p}\right)^{\frac{3}{4}}(GM)^{-\frac{1}{4}}\dot{M}^{-\frac{13}{10}}R_A^{-\frac{9}{4}}\right]$, and $D_3 =$ $\left[\frac{2}{3\pi}\frac{\mu^2}{\mu_0}\left(\frac{243\kappa_0}{512\sigma}\right)^{\frac{1}{10}}\alpha_{ss}^{\frac{4}{5}}\left(\frac{k_B}{\bar{\mu}m_p}\right)^{\frac{3}{4}}(GM)^{-\frac{3}{4}}\dot{M}^{\frac{3}{10}}R_A^{-\frac{23}{4}}\right]$.

Equation (54) is the pressure gradient equation for this model. The first term on the RHS is the dominant term resulting from the difference between the Keplerian and quasi-Keplerian angular momenta. We also note here that the PGF will vanish

in a Keplerian state. This is in agreement with the definition of a thin Keplerian accretion disk (Campbell 1992; Frank et al. 2002). Although pressure is a scalar quantity, PGF is a vector normal to the local disk and is directed along the disk plane.

We plot the PGF in Figure 7 for $P = 7$ s and $P = 100$ s, with varying values of ϵ and ξ. Our results show that the PGF is negative for $\xi = 0.8$, but it becomes positive for $\xi = 1.2$. PGF increases with period, and the local maximum ($\xi = 1.2$) and minimum ($\xi = 0.8$) decrease with increasing radial distance. This reversal translates into torque reversal as the disk makes a transition to and from Keplerian motion. A quasi-Keplerian motion can show observed dynamical scenarios. We shall have a detailed discussion in the next section after finding the net torque acting on the neutron star.

As the disk switches between Keplerianity $\xi = 1.2$ (increased azimuthal velocity) and $\xi = 0.8$ (reduced azimuthal velocity), pressure differences force matter from areas of high pressure to the areas of low pressure; see (Figure 4). Therefore, in addition to magnetic torques, PGF can contribute to the total torque exerted on the neutron star.

3.4. Torques on a Neutron Star in a Quasi-Keplerian Disk

The torques on a neutron star range from magnetic to material; these are obtained from Equations (34) and (52) by multiplying by $2\pi R$ and then vertically integrating from R_{in} to

Table 1
Net Torque on a Neutron Star Evaluated at $R_{\rm in}$

$P_{\rm spin}$	ξ	ϵ	Case	$R_{\rm in}$	$N_{\rm adv}$	$N_{\rm visc}$	$N_{\rm dyn}$	$N_{\rm shear}$	$N_{\rm PGF}$	$N_{\rm Total}$
7.0	0.8	1.0	V	10RA	6.6×10^{26}	-1.2×10^{27}	1.2×10^{27}	-1.7×10^{25}	-7.0×10^{23}	6.4×10^{25}
		0.1	V	2.5RA	3.3×10^{26}	-6.2×10^{26}	7.5×10^{26}	-1.5×10^{26}	-5.6×10^{24}	3.0×10^{26}
		0	V	1.0RA	2.1×10^{26}	-2.0×10^{25}	0	-3.1×10^{26}	-2.2×10^{25}	-1.4×10^{26}
		−0.1	D	2.5RA	3.3×10^{26}	0	-7.5×10^{26}	-1.3×10^{26}	-1.4×10^{25}	-5.6×10^{26}
		−1.0	D	7.0RA	5.5×10^{26}	0	-1.9×10^{27}	-2.9×10^{25}	-6.4×10^{24}	-1.4×10^{27}
	1.0	1.0	V	8.0RA	7.4×10^{26}	-1.4×10^{27}	1.4×10^{27}	-1.9×10^{25}	0	7.2×10^{26}
		0.1	V	2.0RA	3.7×10^{26}	-7.0×10^{26}	8.9×10^{26}	-1.3×10^{26}	0	4.3×10^{26}
		0	V	1.0RA	2.6×10^{26}	-1.5×10^{26}	0	-2.0×10^{26}	0	-9.0×10^{25}
		−0.1	D	2.0RA	3.7×10^{26}	0	-8.9×10^{26}	-1.3×10^{26}	0	-6.5×10^{26}
		−1.0	D	5.7RA	6.2×10^{26}	0	-2.2×10^{27}	-3.1×10^{25}	0	-1.6×10^{27}
	1.2	1.0	V	7.5RA	8.6×10^{26}	-1.6×10^{27}	1.8×10^{27}	-1.8×10^{25}	1.3×10^{24}	1.0×10^{27}
		0.1	V	1.9RA	4.3×10^{26}	-8.1×10^{26}	1.1×10^{27}	-1.1×10^{26}	1.0×10^{25}	6.2×10^{26}
		0	V	1.0RA	3.1×10^{26}	-2.4×10^{26}	0	-1.3×10^{26}	2.7×10^{25}	-3.3×10^{25}
		−0.1	D	1.8RA	4.2×10^{26}	0	-1.2×10^{27}	-1.1×10^{26}	3.1×10^{25}	-8.6×10^{26}
		−1.0	D	5.5RA	7.4×10^{26}	0	-2.7×10^{27}	-2.7×10^{25}	1.3×10^{25}	-2.0×10^{27}
100	0.8	1.0	V	9.5RA	6.5×10^{26}	-1.2×10^{27}	1.3×10^{27}	-1.0×10^{24}	-7.5×10^{23}	7.5×10^{26}
		0.1	V	3.8RA	4.1×10^{26}	-7.7×10^{26}	4.4×10^{27}	-7.8×10^{23}	-3.0×10^{24}	4.0×10^{27}
		0	V	1.0RA	2.1×10^{26}	-3.9×10^{26}	0	2.1×10^{25}	-2.2×10^{25}	-1.8×10^{26}
		−0.1	D	1.8RA	2.8×10^{26}	0	-1.2×10^{27}	2.6×10^{25}	-9.1×10^{24}	-9.0×10^{26}
		−1.0	D	7.0RA	5.5×10^{26}	0	-1.9×10^{27}	-1.4×10^{24}	-6.2×10^{24}	-1.4×10^{27}
	1.0	1.0	V	7.5RA	7.2×10^{26}	-1.3×10^{27}	1.6×10^{27}	-9.3×10^{23}	0	1.0×10^{27}
		0.1	V	2.5RA	4.1×10^{26}	-7.8×10^{26}	8.6×10^{26}	7.9×10^{24}	0	4.8×10^{26}
		0	V	1.0RA	2.6×10^{26}	-4.9×10^{26}	0	2.1×10^{26}	0	-2.0×10^{25}
		−0.1	V	1.0RA	2.6×10^{26}	-1.2×10^{25}	-2.2×10^{27}	2.1×10^{26}	0	-1.7×10^{27}
		−1.0	D	5.5RA	6.1×10^{26}	0	-2.3×10^{27}	-9.4×10^{23}	0	-1.7×10^{27}
	1.2	1.0	V	6.5RA	8.0×10^{26}	-1.5×10^{27}	2.1×10^{27}	-6.7×10^{23}	2.6×10^{24}	1.4×10^{27}
		0.1	V	2.0RA	4.4×10^{26}	-8.3×10^{26}	1.0×10^{27}	2.2×10^{25}	1.5×10^{25}	6.5×10^{26}
		0	V	1.0RA	3.1×10^{26}	-5.9×10^{26}	0	2.2×10^{26}	4.4×10^{25}	-1.6×10^{26}
		−0.1	V	1.0RA	3.1×10^{26}	-2.9×10^{25}	-2.5×10^{27}	2.2×10^{26}	6.4×10^{25}	-1.9×10^{27}
		−1.0	D	4.7RA	6.8×10^{26}	0	-3.3×10^{27}	-1.9×10^{23}	1.6×10^{25}	-2.6×10^{27}

$R_{\rm out}$. The torque contribution from the PGF is:

$$N_{\rm PGF} = -2\pi \int_{R_{\rm in}}^{R_{\rm out}} \Sigma \left[v_R \frac{\partial v_R}{\partial R} - \frac{v_\phi^2}{R} \right] R \, dR$$
$$- 2\pi \int_{R_{\rm in}}^{R_{\rm out}} \frac{\Sigma GM}{R} \, dR$$
$$+ 2\pi \int_{R_{\rm in}}^{R_{\rm out}} \left[\frac{B_z B_R}{\mu_0} \right]_{z=-H}^{z=+H} R \, dR, \qquad (55)$$

where $N_{\rm PGF} = \int_{R_{\rm in}}^{R_{\rm out}} 2\pi R \left(\frac{\partial \Pi}{\partial R} \right) dR$, while the other torques are:

$$[-\xi \dot{M} \sqrt{GMR}]_{R_{\rm in}}^{R_{\rm out}} = \int_{R_{\rm in}}^{R_{\rm out}} \frac{4\pi}{\mu_0} [B_z (B_{\phi,{\rm dyn}} + B_{\phi,{\rm shear}})] R^2 \, dR$$
$$- [3\pi \xi (\nu \Sigma)(GMR)^{\frac{1}{2}}]_{R_{\rm in}}^{R_{\rm out}}, \qquad (56)$$

where $R_{\rm in}$ is the position of the disk's inner edge. The LHS of Equation (56) shows the rate at which angular momentum is transported past the inner and outer edges of the accretion disk, while the first and second terms on the RHS represent the effect of magnetic and viscous stresses, respectively. Considering only the exchange of angular momentum between the neutron star and accretion disk, the torques are obtained as:

$$N_{\rm adv}(r_i) = 2.6 \times 10^{26} \xi \mu_{20}^{2/7} M_1^{3/7} \dot{M}_{13}^{6/7} r_i^{1/2} \qquad (57)$$

$$N_{\rm shear} = -7.5 \times 10^{26} \gamma \mu_{20}^{\frac{2}{7}} M_1^{\frac{3}{7}} \dot{M}_{13}^{\frac{6}{7}} \int_{r_i}^{\infty} \left\{ \frac{1 - (\omega_s/\xi) r^{\frac{3}{2}}}{r^4} \right\} dr \qquad (58)$$

$$N_{\rm dyn} = 1.2 \times 10^{28} \epsilon \gamma_{\rm dyn}^{\frac{1}{2}} \alpha_{\rm ss}^{\frac{1}{20}} \bar{\mu}^{\frac{3}{16}} \mu_{20}^{\frac{1}{4}} M_1^{\frac{5}{8}} \dot{M}_{13}^{\frac{4}{5}} \chi^{-\frac{3}{16}} \int_{r_i}^{\infty} \Lambda^{\frac{17}{40}} r^{-\frac{37}{16}} dr \qquad (59)$$

$$N_{\rm vis}(r_i) = -2.4 \times 10^{27} \xi \mu_{20}^{2/7} M_1^{3/7} \dot{M}_{13}^{6/7} \Lambda(r) r_i^{1/2}. \qquad (60)$$

As the disk deviation from Keplerian motion increases, the magnitude of both shear- ($N_{\rm shear}$) and dynamo-induced ($N_{\rm dyn}$) torques increase. Here, $N_{\rm shear}$ changes sign whenever $\xi > \omega_s$, and the contribution from this torque vanishes at a point when $\xi = \omega_s$. The viscous and advective torques are reduced for $\xi < 1$ and amplified for $\xi > 1$ by 20% below and above the Keplerian case, respectively. The overall effect is that, in the non-Keplerian case, the neutron star experiences torques of greater magnitude than it does for the Keplerian case.

3.5. Assessment of Torque

The total torque exerted on the neutron star, N_T, can be expressed in terms of the inner edge position, $R_{\rm in}$, as:

$$N_T(R_{\rm in}) = N_{\rm PGF} + 2.6 \times 10^{26} \xi r_{\rm in}^{\frac{1}{2}} - 2.5 \times 10^{27} \xi \Lambda_{(r_{\rm in})} r_{\rm in}^{\frac{1}{2}}$$
$$- 3.3 \times 10^{46} \frac{1}{r_{\rm in}^3} \left[1 - \frac{2}{\xi} \left(\frac{r_{\rm in}}{r_{\rm co}} \right)^{\frac{3}{2}} \right]$$
$$+ 5.2 \times 10^{42} \epsilon \Lambda_{(r_{\rm in})}^{\frac{17}{40}} r_{\rm in}^{-\frac{21}{16}}. \tag{61}$$

Here, $\Lambda_{R_{\rm in}}$ means evaluation at $R_{\rm in}$. The range from $R_{\rm in}$ to ∞ covers both spin-up and spin-down contributions from magnetic stresses. Specifically, $R_{\rm in} \to R_{\rm co}$ results in a spin-up torque, while $R_{\rm co} \to \infty$ contributes a spin-down torque to the neutron star (Wang 1987, 1995).

Numerical solutions for torques arising due to interaction of the neutron star and accretion disk are calculated and tabulated in Table 1.

From Table 1, we see that there is a torque reversal for $\xi > 1$ and $\xi < 1$. This results from the PGF changing direction whenever the disk transits to or from quasi-Keplerianity. For $\xi = 0.8$, the PGF is directed away from the star, resulting into a negative torque that couples with viscous torque. This coupled torque is responsible for transporting angular momentum outward from the neutron star. On the other hand, when $\xi = 1.2$, the azimuthal velocity is faster and the positive PGF (directed toward the star) torque is coupled with the advective torque. In this case, angular momentum is advected out of the inner edge of the accretion disk, causing the star to spin up. Both $N_{\rm adv}(R_{\rm in})$ and $N_{\rm vis}(R_{\rm in})$ can result in warping of the disk (Scott & Shane 2014).

Additionally, in a quasi-Keplerian system, the internal dynamo generated torque is observed to be dominant when $\epsilon \neq 0$. This is in agreement with the findings of Tessema & Torkelsson (2010) for a purely Keplerian disk model with a dynamo. When $\epsilon = 0$, $N_{\rm PGF}$ makes a significant contribution to the total torque. Thus, our mechanism can account for the observed enhanced torque reversals in some astronomical environments.

3.6. Comparison with Observational Results

Torque reversal from spin-up to spin-down of a neutron star is a common phenomenon. It occurs in systems like 4U 1626-67, which is observed to have a spin-up/-down rate $\dot{\nu}$ as $+8.5 \times 10^{-13}/-7.0 \times 10^{-13}$ Hz s^{-1} at a spin period of 7.6 s (Camero-Arranz et al. 2010). Further, 4U 1728-247 has a spin-up/-down rate of $\dot{\nu}$ as $+6.0 \times 10^{-12}/-3.7 \times 10^{-12}$ Hz s^{-1} at a spin period of 120 s (Bildsten et al. 1997). These spin variations are related to torque, $N_{\rm Total}$, as:

$$\dot{\nu} = \frac{N_{\rm Total}}{2\pi I}, \tag{62}$$

where $\dot{\nu}$ is the rate of spin change measured in Hz s^{-1}, and I is the moment of inertia of the neutron star defined as

$$I = \frac{2}{5} M_s R_s^2. \tag{63}$$

The observed spin-up/-down rates are in agreement with the result of our model in Table 1 for a neutron star with a radius $R_s = 10$ km (Frank et al. 2002).

4. Conclusion

We have obtained a complete structure of a quasi-Keplerian model where the magnetic field dynamo forms a part. In this model, we argue that pressure gradient is not negligible, whereas previous models assumed it was. Our results show that, at large radii, the disk remains Keplerian, while inside a critical radius, the rotation is quasi-Keplerian. While in this state, the accretion disk can make a transition to and from a Keplerian fashion. The corotation radius is shifted inward (outward) for $\xi > 1$ (for $\xi < 1$), and the position of the inner edge with respect to the new corotation radius is also relocated accordingly as compared to the Keplerian model. The resulting torques are of greater magnitude compared to the Keplerian model. The interesting part, found in a quasi-Keplerian model, is that PGF torque couples with viscous torque (when $\xi < 1$) to provide a spin-down torque and a spin-up torque (when $\xi > 1$) by coupling with the advective torque. This enhanced torque reversal is important in explaining the observed variations in spin frequency of accretion-powered systems like 4U 1626-67. Further, the dynamo action is in conformity with previous results, except that $N_{\rm dyn}$ is of increased magnitude in a quasi-Keplerian model. This result is a breakthrough because finding a complete structure for a quasi-Keplerian disk model has not always been successful (e.g., Hoshi & Shibazaki 1977).

ORCID iDs

Isaac Habumugisha ⬤ https://orcid.org/0000-0002-2544-0219

References

Bakala, P., Sramkova, E., Stuchlik, Z., & Torok, G. 2010, CQGra, 27, 045001
Bildsten, L., Chakrabarty, D., Chiu, J., et al. 1997, ApJS, 113, 367
Brandenburg, A., Nordlund, A., Stein, R. F., & Torkelsson, U. 1995, ApJ, 446, 741
Burderi, L., Di Salvo, T., Menna, M. T., Riggio, A., & Papitto, A. 2006, ApJL, 653, L133
Camero-Arranz, A., Finger, M. H., Ikhsanov, N. R., Wilson-Hodge, C. A., & Beklen, E. 2010, ApJ, 708, 1500
Campbell, C. G. 1987, MNRAS, 229, 405
Campbell, C. G. 1992, GApFD, 63, 179
Campbell, C. G. 1999, GApFD, 90, 113
Campbell, C. G., & Heptinstall, P. M. 1998, MNRAS, 299, 31
Elsner, R. F., & Lamb, F. K. 1977, ApJ, 215, 897
Frank, J., King, A., & Raine, D. 2002, Accretion Power in Astrophysics (Cambridge: Cambridge Univ. Press)
Ghosh, P., & Lamb, F. K. 1978, ApJL, 223, L83
Ghosh, P., & Lamb, F. K. 1979a, ApJ, 232, 259
Ghosh, P., & Lamb, F. K. 1979b, ApJ, 234, 296
Hoshi, R., & Shibazaki, N. 1977, PThPh, 58, 1759
Lai, D. 1998, ApJ, 502, 721
Lai, D. 1999, ApJ, 524, 1030
Narayan, R., & Yi, I. 1995, ApJ, 452, 710
Naso, L., & Miller, J. C. 2010, A&A, 521, A31
Naso, L., & Miller, J. C. 2011, A&A, 531, A163

Petri, J. 2013, MNRAS, 433, 986
Petri, J. 2014, MNRAS, 439, 1071
Rezzolla, L., Ahmedov, B. J., & Miller, J. C. 2001, MNRAS, 322, 723
Scott, T., & Shane, W. D. 2014, MNRAS, 441, 1408
Shakura, N. I., & Sunyaev, R. A. 1973, A&A, 24, 337
Shakura, N. I., & Sunyaev, R. A. 1976, MNRAS, 175, 613

Tessema, S. B., & Torkelsson, U. 2010, A&A, 509, A45
Tessema, S. B., & Torkelsson, U. 2011, MNRAS, 412, 1650
Torkelsson, U. 1998, MNRAS, 298, L55
Wang, Y. M. 1987, A&A, 183, 257
Wang, Y. M. 1995, ApJ, 449, L153
Yi, I., Wheeler, J. C., & Vishniac, E. T. 1997, ApJ, 481, L51